Emergent Gravitational Scaling and Quasi-Dark Matter from Quantum Central Limit Theorem Coarse-Graining

Tien D. Kieu *

Posted Date: 19 March 2026

doi: 10.20944/preprints202603.1532.v1

Keywords: quantum central limit theorem

 doi:10.20944/preprints202603.1532.v1

Article

Emergent Gravitational Scaling and Quasi-Dark Matter from Quantum Central Limit Theorem Coarse-Graining

Tien D. Kieu

Centre for Quantum Technology Theory, and Optical Sciences Centre, Swinburne University of Technology, Australia; tdkieu@swin.edu.au

Abstract

The Quantum Central Limit Theorem (QCLT) governs the emergence of classical behaviour in large ensembles of identical quantum subsystems through self-averaging of collective observables. For nonlinear observables, however, the strict inequality $\langle f(\hat{A})\rangle \neq f(\langle\hat{A}\rangle)$ generates residual corrections that survive coarse-graining at subleading order and persist into the classical regime. We analyse the consequences of this structure for macroscopic quantum systems evolving in a Newtonian gravitational potential. Applying the QCLT to the collective centre-of-mass dynamics of a large ensemble of identical subsystems, we show via the Ehrenfest theorem that the effective force law acquires an additional term proportional to $\langle r^{-2}\rangle - \langle r\rangle^{-2}$, which is strictly non-vanishing by Jensen's inequality whenever the radial distribution has finite variance. We develop the mixed-state construction at three levels of generality. No modification of the gravitational interaction nor new matter fields are introduced; the effect arises solely from nonlinear expectation-value algebra under quantum coarse-graining. This framework leads to emergent enclosed-mass scaling $\Delta M(R)/M_b \sim R/\kappa$ (quasi-dark matter) for $\kappa \ll R \ll R_{\rm corr}$, corresponding to an isothermal effective density profile $\rho_{\rm quasi} \propto R^{-2}$ and a logarithmic gravitational potential $\Phi(R) \propto \ln(R/R_0)$. This reproduces flat galactic rotation curves and the baryonic Tully–Fisher relation $V_{\rm flat} \propto M_b^{1/4}$, with the onset of flattening predicted at $R \sim \kappa \propto \sqrt{M_b/\Sigma_0}$, a galaxy-by-galaxy falsifiable prediction absent from both ΛCDM and MOND. The framework further predicts a surface-density-dependent Radial Acceleration Relation, $g_{\rm obs} \propto \sqrt{G\Sigma_0}\,\sqrt{g_{\rm bar}}$, testable against the SPARC dataset.Beyond $R_{\rm corr}$, identified with the HI truncation radius, the correction saturates and Keplerian decline is restored. Relativistic extensions and cosmological implications are left for future work. These results demonstrate that quantum statistical coarse-graining alone can generate nontrivial emergent scaling behaviour at macroscopic scales, and highlight a structural link between limit theorems in many-body quantum mechanics and emergent classical dynamics.

Keywords: quantum central limit theorem

1. Introduction

The evidence for dark matter (see the recent extensive review [1] and references therein) is overwhelming with galactic rotation curves remain flat at large radii, galaxy clusters display excess gravitational binding, and large-scale structure formation requires additional gravitating mass. Yet, despite decades of effort, no dark matter particle has been directly and conclusively detected, and the Standard Model of particle physics offers no natural candidate. This persistent absence of detection motivates the search for alternative explanations.

One compelling avenue is to reconsider the nature of gravity itself. Alternative frameworks include Modifications of Newtonian Dynamics (MOND) and relativistic extensions [2,3] have been proposed, but these often require ad hoc assumptions or introduce tensions with cosmological data [4]; emergent gravity [5]; and quantum-inspired mechanism [6–8]. See also [9] for a recent review covering multiple approaches.

 doi:10.20944/preprints202603.1532.v1

In this work, we explore the possibility that *dark matter effects are emergent*, arising from quantum fluctuations at large scales through the *Quantum Central Limit Theorem* (QCLT) [10].

For a macroscopic body consisting of $N \gg 1$ identical quantum subsystems — such as neutral hydrogen atoms in the outer disk — QCLT describes the emergence of classical, coarse-grained dynamics. Crucially, this emergence is imperfect: for nonlinear observables, quantum expectation-value corrections survive the coarse-graining limit. In a gravitational field, such correction generates an effective additional force indistinguishable observationally from that of a dark matter halo – a kind of *quasi–dark matter*. In this work we derive this correction explicitly, demonstrate that it reproduces the baryonic Tully Fisher relation and flat rotation curves, and identify some new, falsifiable predictions: the dependence of the rotation-curve flattening radius, Tully–Fisher normalisation, and Radial Acceleration Relation on the central baryonic surface density Σ_0 — predictions that are absent from both ΛCDM and MOND.

Throughout, we restrict to non-relativistic, galactic-scale dynamics traced by dynamically cold neutral hydrogen at intermediate radii, where dynamically cold baryonic tracers are present. Gravitational lensing and CMB constraints require a covariant extension left for future work.

In the next section, we state the Quantum Central Limit Theorem. Following from that is a consideration of its consequences on a macroscopic object consisting of a large number of identical and non-interacting subsystems in a gravitational field. We demonstrate specifically that a quantum-induced quasi–dark matter term modifies the effective radial force law, yielding various testable astrophysical predictions. Following that are discussions on various aspects and implications of our approach. We then conclude the paper with some remarks.

2. Quantum Central Limit Theorem

Consider a collective system of mass m consisting of N subsystems, which are non-interacting and identical (coherence is not required). Each of the subsystem has mass μ and is in an identical state $|\phi\rangle$ governed by a Hamiltonian $H_\mu(\hat{x}, \hat{p})$. Let $\hat{X}$ be the centre of mass, and $\hat{V}$ the velocity of the centre of mass, and $|\Phi\rangle$ the state of the collective system,

$$\begin{aligned} \hat{X} &= \frac{1}{N}\sum_{i=1}^{N} \hat{x}_i, \\ \hat{V} &= \frac{1}{N}\sum_{i=1}^{N} \frac{\hat{p}_i}{\mu} := \frac{1}{N}\sum_{i=1}^{N} \hat{v}_i, \\ |\Phi\rangle &= \bigotimes_{i=1}^{N} |\phi_i\rangle, \end{aligned} \tag{1}$$

where $|\phi_i\rangle = |\phi\rangle$ for all i.

For a *Hermitian* combination of some finite sum of products of $\hat{X}$ and $\hat{V}$ to obtain, for $N \gg 1$, we have the following result [10]

$$\begin{aligned} \left\langle\left\langle \sum_{mn} (c_{mn} X^m V^n + c^*_{mn} V^n X^m) \right\rangle\right\rangle &:= \left\langle \Phi \middle| \sum_{mn} (c_{mn} X^m V^n + c^*_{mn} V^n X^m) \middle| \Phi \right\rangle, \\ &= \int dX dV \left(2 \sum_{mn} \Re(c_{mn}) X^m V^n \right) \mathcal{P}_{re}(X, V) \\ &\quad + \int dX dV \left(\sum_{mn} \Im(c_{mn}) X^m V^n \right) \mathcal{P}_{im}(X, V). \end{aligned} \tag{2}$$

In this work we only need the expectation values for single operators X and V. For self-containment, we derive these required results (A11) and (A12) in Appendix A, with f and g are some suitable functions,

 doi:10.20944/preprints202603.1532.v1

$$\begin{aligned}\left\langle \Phi \middle| f\left(\frac{1}{N}\sum_i^N \hat{x}_i\right) \middle| \Phi \right\rangle &\overset{N\to\infty}{\longrightarrow} f(\langle x\rangle),\\ \langle \Phi | g(\hat{P}/m) | \Phi \rangle &\overset{N\to\infty}{\longrightarrow} g(\langle p\rangle/\mu).\end{aligned} \tag{3}$$

where we have defined for subsystem with pure state $\hat{\rho} = |\phi\rangle\langle\phi|$, for $\hat{a} = \hat{x}$ or $\hat{v}$,

$$\begin{aligned}\langle \hat{a} \rangle &:= tr(\hat{a}\hat{\rho}),\\ \sigma_a^2 &:= tr(\hat{a}^2\hat{\rho}) - tr(\hat{a}\hat{\rho})^2.\end{aligned}$$

These can be generalised to mixed states with weights $0 < \omega < 1$,

$$\hat{\rho} = \omega|\zeta\rangle\langle\zeta| + (1-\omega)|\eta\rangle\langle\eta|.$$

A regime of classicality hence emerges for the coarse-grained due to the fact that quantum correlations and all traces of quantum behaviours are now suppressed, except those inherent in the quantum expectation values $\langle x\rangle$ and $\langle v\rangle$. This latter is a crucial element that we will make use of in the next section.

3. Ehrenfest Dynamics and Nonlinear Expectation Values in a Gravitational Field

Neutral Hydrogen gas HI in the galactic reservoir provides dynamically cold tracers whose orbital velocities reveal the effective gravitational field, and is therefore a suitable candidate for the application of QCLT.

The Hamiltonian for a single system of mass μ in the (background) gravitational field generated by a body of baryonic mass M_b is

$$H_\mu = \frac{p^2}{2\mu} - \frac{GM_b\mu}{r}. \tag{4}$$

Let $\vec{P}_m$ be the centre-of-mass momentum vector of the collective body of mass m. According to the QCLT of the last section, we can derive the following relationship generalised to three dimensions,

$$\langle\langle \vec{P}\rangle\rangle_m := \left\langle \Phi \middle| \vec{P} \middle| \Phi \right\rangle = \frac{m}{\mu}\langle\vec{p}\rangle_\mu, \tag{5}$$

where the double brackets denote the expectation value for the collective body and $\langle\vec{p}\rangle_\mu$ is the expectation value of the momentum vector of a single subsystem, which has exactly the same mathematics as that of the non-relativistic Hydrogen atom but with the gravitational interactions replacing the electrical interactions. As an estimate for a typical spiral galaxy, $N \sim m_{\mathrm{HI}}/\mu_{\mathrm{H}} \sim (10^9 M_\odot)/(1.67\times10^{-27}kg) \sim 10^{60}$. This confirms the $N\to\infty$ limit is extremely well satisfied for an application of QCLT.

We can then calculate from (5) the gravitational force acting on the collective body by taking the time derivative of the collective momentum. Applying the Ehrenfest theorem

$$\begin{aligned}\langle\langle \vec{F}\rangle\rangle_m &= \frac{d}{dt}\langle\langle\vec{P}\rangle\rangle_m,\\ &\overset{(5)}{=} \frac{m}{\mu}\frac{d}{dt}\langle\vec{p}\rangle_\mu,\\ &\overset{\text{Ehrenfest}}{=} \frac{m}{\mu}\frac{1}{i\hbar}\langle[\vec{p}, H_\mu]\rangle_\mu,\\ &\overset{(4)}{=} -GM_b m\left\langle\frac{\vec{r}}{r^3}\right\rangle_\mu.\end{aligned} \tag{6}$$

 doi:10.20944/preprints202603.1532.v1

One might note that a classical density distribution $\rho_{\text{sub}}(r)$, for the subsystem, would equally produce

$$\langle 1/r^2 \rangle = \int \frac{\rho_{\text{sub}}(r)}{r^2}\, dr.$$

However, the crucial point is the inequality

$$\langle 1/r^2 \rangle - \frac{1}{\langle r \rangle^2} \neq 0, \tag{7}$$

which survives coarse–graining and enters the Ehrenfest equation. This is a critical result whose logical consequences will be explored next.

4. Mixed-State Construction and Emergent Mass Scaling - Quasi-Dark Matter

From large-scale observations of the universe, discrepancies have been found in the observable ordinary/baryonic matter and their gravitational effects. Dark matter is then hypothesised to account for these discrepancies.

Let $M_b(R)$ be the mass of baryonic matter and $\Delta M(R)$ be that of hypothesised dark matter, both of which can be a function of R. Then the non-relativistic gravitational pull on a collective body of mass m in the radial component is $-G(M_b + \Delta M(R))m/R^2$.

Here, we pursue instead the logical and mathematical consequences of (6) and equate the force with the QCLT force in the last Section, with $\Delta M(R)$ now the quantum-induced quasi dark matter,

$$\begin{aligned} \vec{F}|_{radial} &= -G(M_b + \Delta M(R))m/R^2, \\ &\overset{\text{QCLT}}{=} -G(M_b + \Delta M(R))m/\langle r \rangle_\mu^2, \\ &\overset{(6)}{=} -GM_b m\langle 1/r^2 \rangle_\mu, \end{aligned} \tag{8}$$

since it can be shown from the QCLT for the centre of mass R (3) that $1/R^2 = \langle\langle 1/R^2 \rangle\rangle_m = 1/\langle r \rangle_\mu^2$. We thus obtain

$$\frac{\Delta M(R)}{M_b} = \left(\left\langle \frac{1}{r^2} \right\rangle_\mu - \frac{1}{\langle r \rangle_\mu^2} \right) \langle r \rangle_\mu^2. \tag{9}$$

For the expectation values, we consider in this Section an entangled state between the states of a subsystem with its corresponding environment and then trace out the environment to obtain a mixed state. Consider the pure entangled state of a system S and its environment E,

$$|\Psi_{SE}\rangle = \sqrt{\omega}\,|E_1\rangle \otimes |\psi_R\rangle + \sqrt{1-\omega}\,|E_2\rangle \otimes |\psi_\kappa\rangle, \tag{10}$$

where $\langle E_1|E_2\rangle = 0$ and $0 \leq \omega \leq 1$. The two states $|\psi_R\rangle$ and $|\psi_\kappa\rangle$ are respectively associated with two different scales R and κ. The total density matrix is $\rho_{SE} = |\Psi_{SE}\rangle\langle\Psi_{SE}|$. Tracing over the environment yields

$$\hat{\rho}_S = \text{Tr}_E(\hat{\rho}_{SE}) = \omega\,|\psi_R\rangle\langle\psi_R| + (1-\omega)\,|\psi_\kappa\rangle\langle\psi_\kappa|, \tag{11}$$

since the cross terms vanish due to $\langle E_1|E_2\rangle = 0$. Hence, even though the total system is in a pure state, the subsystem S is described by a statistical mixture.

We explicitly construct in Appendix B a family of some explicit quantum mixed states with Gamma distributions $\Gamma(r;\alpha,\beta)$,

$$r^2\langle r|\hat{\rho}_S|r\rangle \quad \longrightarrow \quad \omega\Gamma(r;\alpha_1,\beta_1) + (1-\omega)\Gamma(r;\alpha_2,\beta_2), \tag{12}$$

 doi:10.20944/preprints202603.1532.v1

such that we can obtain, from (A20) and (A21), with R-dependent weight $\omega(R)$,

$$\langle r \rangle_\mu \quad \overset{\kappa \ll R}{\longrightarrow} \quad R + o(R), \tag{13}$$

$$\frac{M_b + \Delta M(R)}{M_b} \quad \overset{\kappa \ll R \ll R_{\rm corr}}{=} \quad \left\langle \frac{1}{r^2} \right\rangle_\mu \langle r \rangle_\mu^2 \longrightarrow \frac{R}{\kappa} + o(R), \tag{14}$$

for some scaling distance κ given in (A22), which is dictated by the physics of the system, and $R_{\rm corr}$ represents the characteristic correlation length of neutral hydrogen reservoir, which will be discussed in the next section. QCLT framework thus produces an emergent large-scale force correction with similar radial scaling as dark matter halos.

It is important to recognise that we need different states $\hat{\rho}$ in (12) at different distances R, that is, $\hat{\rho} = \hat{\rho}(R)$. Such distance dependence resides in the dependence on R for the weights $\omega = \omega(R)$, and for the pure state components of the mixed state (12). See Appendix B for more details.

The dependency is a physically motivated ansatz. Consider a hydrogen atom at galactocentric radius R in the outer disk. It is weakly coupled to the interstellar radiation field and nearby matter. Standard open-system quantum mechanics (Lindblad equation) describes the reduced density matrix of each atom after tracing out the environment. In the outer disk, the mean free path and the correlation length of the radiation field both scale with R (lower density, longer correlation lengths). One therefore expects the off-diagonal coherence between macroscopically separated states — those localised near the galactic centre, $|\psi_\kappa\rangle$, and those at the current radius, $|\psi_R\rangle$ — to be suppressed as $(\kappa/R)^\alpha$ for some $\alpha > 0$. The simplest case $\alpha = 1$ gives $\omega(R) = 1 - c/R$ exactly. This is not merely an ansatz; it is motivated from a decoherence model in which the pointer states are radially localised and the environment provides thermal photons with the HI mean free path $l_{\rm coh} \sim R$.

The effective contribution arises from the R–dependence of the mixed state $\hat{\rho}(R)$ and not from any modification of the gravitational interaction itself. No projective measurement or wavefunction collapse is invoked; only expectation values enter the dynamics. This amounts to an effective density distribution for quasi-dark matter which is iso-thermal like,

$$\begin{aligned} \rho_{\rm quasi}(R) &= \frac{1}{4\pi R^2} \frac{d(\Delta M)}{dR}, \\ &\propto 1/R^2, \end{aligned} \tag{15}$$

a significant advantage over both ΛCDM (which inputs a halo profile) and MOND (which modifies dynamics globally).

Ultimately, as the total number of subsystems N is a function of R, the density of quantum subsystems (hydrogen atoms) falls off with radius. Then the QCLT applicability weakens as $N(R)$ decreases, and the "classicality" emergence may be incomplete.

It is important to note that apart from our explicit state construction (12), there might exist other different quantum states that can also lead to the behaviour in (14).

 doi:10.20944/preprints202603.1532.v1

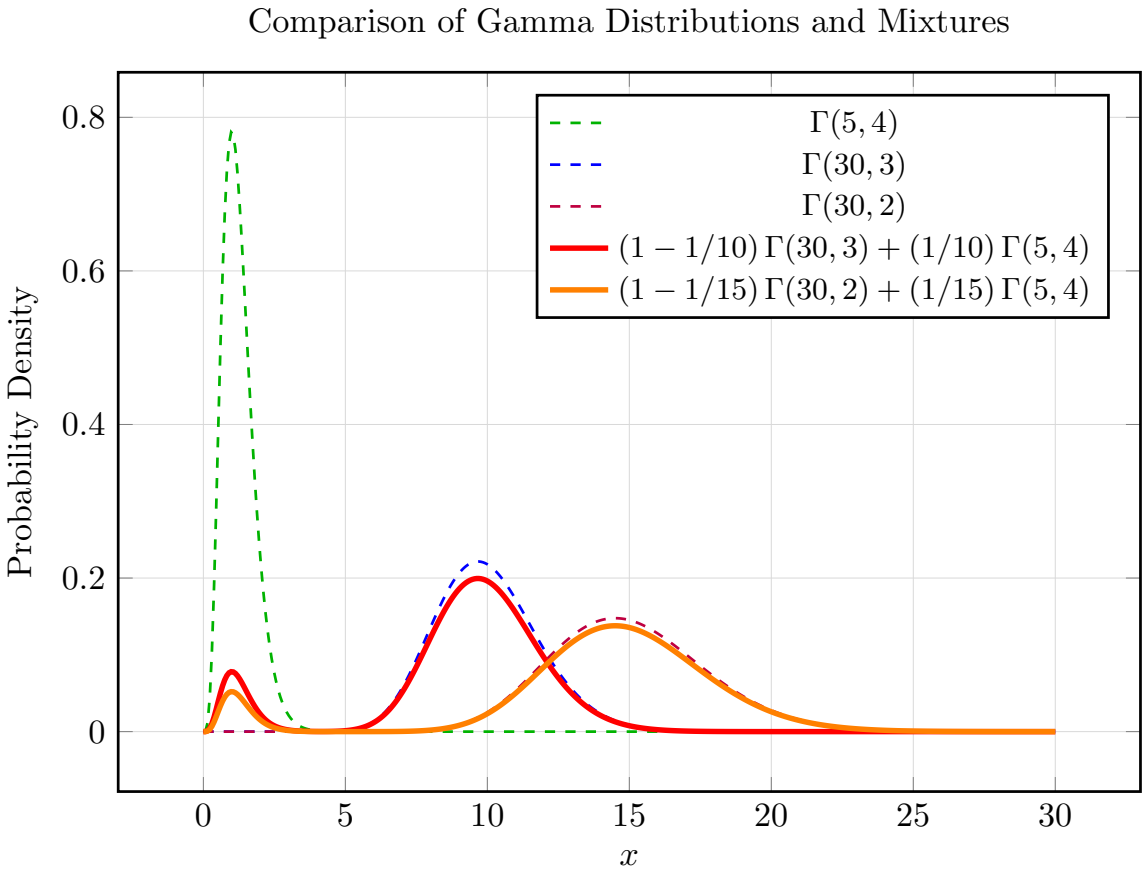

Figure 1. Examples of mixtures of two Gamma distributions.

5. Generalisation to Tweedie Distributions

5.1. Rationale and Physical Motivation

The mixed-state construction of Appendix B employs a two-component mixture of Gamma distributions with an R-dependent weight $\omega(R) = 1 - c/R$ to achieve the asymptotic scaling $\Delta M(R)/M_b \sim R/\kappa$. While this construction is explicit and mathematically controlled, it raises a natural question: is the result specific to the Gamma family, or does it belong to a broader and more fundamental class of distributions?

We show here that the answer is the latter. The Gamma distribution is the $p = 2$ member of the *Tweedie family* of exponential dispersion models [11–13], a one-parameter class characterised by a power-law variance–mean relation. Three independent lines of reasoning motivate this generalisation.

(i) The hydrogen eigenstate wavefunctions.

The subsystem Hamiltonian (4) shares the mathematics of the hydrogen atom, whose radial probability densities in eigenstate $|n, \ell\rangle$ take the form

$$|\psi_{n\ell}(r)|^2 \propto r^{2\ell+2}\, e^{-r/(na_0)} \left[L^{2\ell+1}_{n-\ell-1}(2r/na_0)\right]^2, \tag{16}$$

where L^{α}_{k} denotes an associated Laguerre polynomial and a_0 the Bohr radius (here replaced by the gravitational analogue). For the s-wave ($\ell = 0$) states, the squared modulus reduces to a Gamma distribution, as used in Appendix B. For states with $\ell > 0$, the additional factor $r^{2\ell}$ and the Laguerre polynomial structure produce radial distributions that belong to the compound Poisson–Gamma subfamily of Tweedie models, $1 < p < 2$, and to the Inverse Gaussian subfamily $p = 3$ for specific combinations of quantum numbers. A mixed state $\hat{\rho}(R)$ constructed from a realistic ensemble of

 doi:10.20944/preprints202603.1532.v1

hydrogen eigenstates therefore naturally samples the full Tweedie family rather than the Gamma subfamily alone.

(ii) The decoherence model.

The physical motivation for $\omega(R) = 1 - c/R$ developed in Section 4 invokes open-system dynamics described by the Gorini–Kossakowski–Sudarshan–Lindblad (GKSL) master equation [14,15]. This master equation can be transformed into a quantum Fokker–Planck equation for quasi-probability distributions [16]. When the system–environment coupling is position-dependent—as expected in the outer disk, where the mean free path and radiation correlation length both scale with R—the diffusion coefficient of the resulting Fokker–Planck equation acquires a power-law dependence on the radial coordinate. It is well established that Fokker–Planck equations with power-law diffusion coefficients $D(r) \propto r^{\alpha}$ admit steady-state distributions whose variance scales as a power law in the mean, $\mathrm{Var}(r) \propto \mu^{p}$ with p determined by α [17]. While a complete derivation of the steady-state Tweedie index from first principles of the galactic radiation field lies beyond the scope of this work, the chain of reasoning—GKSL master equation $\to$ quantum Fokker–Planck $\to$ power-law diffusion $\to$ Tweedie attractor—is physically well motivated and each step individually supported [16–18].

5.2. The Tweedie Family

An exponential dispersion model $\mathrm{Tw}_p(\mu, \phi)$ with mean μ, dispersion parameter $\phi > 0$, and Tweedie power index p has the variance function

$$\mathrm{Var}(r) = \phi\, \mu^{p}. \tag{17}$$

The family is defined for $p \in (-\infty, 0] \cup [1, \infty)$, and the following subfamilies are of particular relevance:

$$\begin{aligned} p = 0: &\quad \text{Normal (Gaussian)},\\ p = 1: &\quad \text{Poisson},\\ p = 2: &\quad \text{Gamma } \Gamma(r;\alpha,\beta), \quad \mu = \alpha/\beta,\ \phi = 1/\alpha,\\ 1 < p < 2: &\quad \text{Compound Poisson–Gamma},\\ p = 3: &\quad \text{Inverse Gaussian IG}(\mu,\lambda), \quad \phi = 1/\lambda. \end{aligned} \tag{18}$$

For $p \notin \{0, 1, 2, 3\}$, no closed-form density exists in general, though series representations are available [19].

The Inverse Gaussian distribution ($p = 3$) has probability density

$$f(r;\mu,\lambda) = \sqrt{\frac{\lambda}{2\pi r^3}}\, \exp\!\left(-\frac{\lambda(r-\mu)^2}{2\mu^2 r}\right), \quad r > 0, \tag{19}$$

with moments

$$\mathbb{E}[r] = \mu, \qquad \mathrm{Var}(r) = \frac{\mu^3}{\lambda}. \tag{20}$$

It was derived independently by Schrödinger [20] and Smoluchowski [21] as the first-passage time distribution of Brownian motion with drift: the distribution of the time for a particle undergoing diffusion with drift velocity v to first reach a boundary at distance d, with $\mu = d/v$ and $\lambda = d^2/D$ where D is the diffusion coefficient.

The Inverse Gaussian parameter λ has a direct physical interpretation as a diffusion–drift ratio, as in the Brownian motion analogy [20–22].

Figure 2 depicts the contributions from the Inverse Gaussian distributions. Further discussions on the Tweedie distributions are presented in Appendix C.

 doi:10.20944/preprints202603.1532.v1

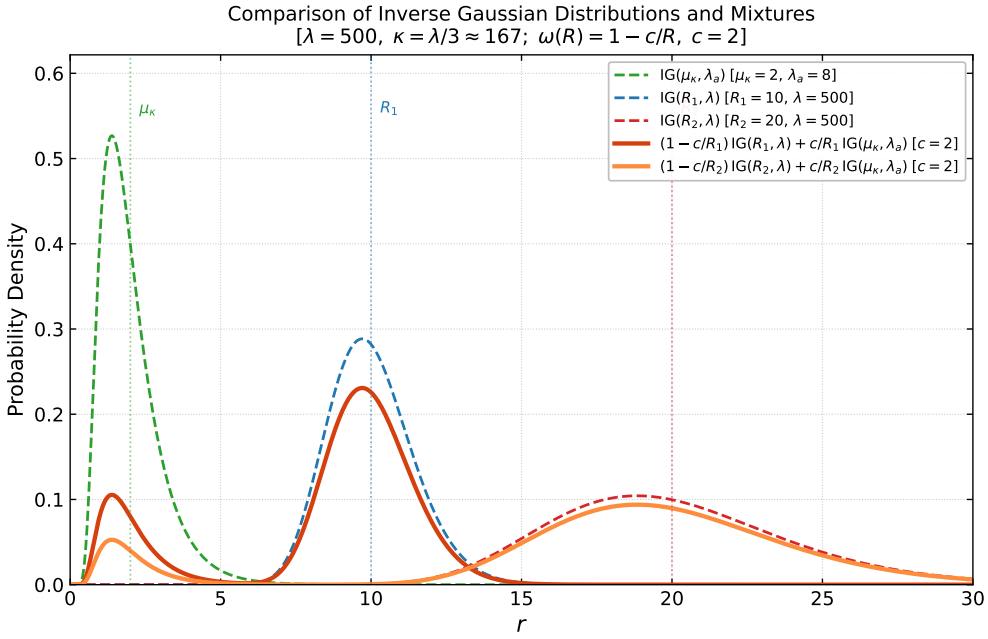

Figure 2. Examples of mixtures of two Inverse Gaussian distributions, $\omega(R)\,\mathrm{IG}(R,\lambda) + [1-\omega(R)]\,\mathrm{IG}(\mu_\kappa,\lambda_a)$, with R-dependent weight $\omega(R) = 1 - c/R$, for two values of the galactocentric radius R. The *bulk component* (blue and red dashed curves) has mean $\mu = R$ and fixed shape parameter $\lambda = 500$. The *anchor component* (green dashed curve) is centred at the inner structural scale $\mu_\kappa = 2$ with $\lambda_a = 8$; it represents the small-scale quantum states localised near the galactic centre, analogous to the state $|\psi_\kappa\rangle$ in Equation (10). The mixture weight on the anchor, $(1-\omega(R)) = c/R$ with $c = 2$, decays with increasing R, so the anchor contribution—visible as a shoulder near $r \approx 2$—weakens as the galactocentric radius grows, consistent with the decoherence model of Section 4. The progressive broadening of the bulk component with R reflects the Inverse Gaussian variance law, $\mathrm{Var}(r) = R^3/\lambda \propto \mu^3$, which is the defining property of the Tweedie $p = 3$ subfamily (cf. Equation (17)). This μ^3 scaling of the variance is precisely the mechanism that generates a Jensen correction $\langle r^{-2}\rangle - \langle r\rangle^{-2} \propto R^{-1}$ (Equation (A32)), and hence an emergent quasi-dark mass $\Delta M(R)/M_b \propto R$ (Equation (A33)), corresponding to flat rotation curves. Compare with Figure 1, which shows the analogous construction using Gamma distributions ($p = 2$); the linear quasi-dark mass scaling there requires an explicit R-dependent mixture weight, whereas here it follows directly from the $p = 3$ variance structure of a single Inverse Gaussian.

6. Astrophysical Implications

6.1. Rotational Curves

Observations of many galaxies of different sizes and structures indicate that the rotational curves apparently remain flat for large distances R from the galactic centres, instead of the Keplerian decrease $\sim 1/\sqrt{R}$ —as in the observations of the 21 cm line emission from neutral hydrogen gas in spiral galaxies [23–25].

QCLT, on the other hand, can offer an alternative framework. In this framework, the effective dynamics arises from tracing out environmental degrees of freedom from an underlying pure quantum state. The residual subsystem evolves according to an effective potential that depends on a characteristic length scale κ. It can then reproduce the fact that the orbital velocity $V(R)$ tends to flatten at large radii, where the visible baryonic mass density has already declined, before decreases according to Keplerian law.

To show that, we equate the galactic centripetal force, which has orbital velocity V, with the gravity attraction (8),

$$\vec{F}|_{radial} \quad = \quad mV^2/R = G(M_b + \Delta M(R))m/R^2, \tag{21}$$

 doi:10.20944/preprints202603.1532.v1

from which,

$$V \xrightarrow{R\gg\kappa} \sqrt{G\,M_b/\kappa}. \tag{22}$$

This is a flatenning of the rotational velocity curve.

6.2. Domain of Validity and Saturation of the Quantum-Induced Contribution

The linear growth of the quantum-induced quasi–dark contribution derived in Equation (12) should be understood as an intermediate–asymptotic regime, rather than a statement about arbitrarily large galactocentric radii. The construction of the effective mixed state $\rho(R)$, and in particular the scaling $\omega(R) = 1 - c/R$ in (A18), relies on the applicability of the QCLT coarse-graining to a large ensemble of effectively identical, dynamically cold subsystems embedded in a stable environment. These conditions necessarily hold only over a finite radial range.

We therefore make explicit the domain of validity of the asymptotic scaling as

$$\boxed{\kappa \ll R \ll R_{\rm corr},} \tag{23}$$

where κ is the intrinsic structural scale introduced in Equation (9), and $R_{\rm corr}$ denotes a correlation radius beyond which the self–averaging assumptions required for QCLT coarse–graining cease to apply. (For example, for HI truncation at 4–6 R_d with $R_d \sim 3$ kpc, one has $R_{\rm corr} \sim 12\tilde{}18$ kpc.) Beyond this radius, the effective mixture parameters saturate,

$$\omega(R) \xrightarrow{R\gg R_{\rm corr}} \omega_\infty\,, \tag{24}$$

implying that the quantum-induced contribution no longer grows with R.

As a result, the effective quasi–dark mass and rotational velocity behave as

$$\Delta M(R) \xrightarrow{R\gg R_{\rm corr}} \Delta M_\infty, \qquad V(R) \sim R^{-1/2}, \tag{25}$$

restoring an asymptotically Keplerian decline at sufficiently large distances. The observed flattening of galactic rotation curves is therefore interpreted as a robust intermediate-scale phenomenon rather than an asymptotic property extending to infinity.

Observationally, extended rotation curves are predominantly traced by dynamically cold neutral hydrogen (HI). Numerous studies indicate that HI surface densities decline sharply beyond $\Sigma_{\rm HI} \sim 1\,M_\odot\,{\rm pc}^{-2}$, typically at radii $R \sim (4-6)\,R_d$, where R_d is the exponential disk scale length. Beyond this regime, ionisation, loss of coherence, and environmental coupling become significant.

Within the present framework, this transition naturally corresponds to the breakdown of the conditions required for QCLT coarse–graining. We therefore identify the HI truncation scale with the correlation radius $R_{\rm corr}$, without invoking a sharp cutoff or introducing additional dynamical assumptions. No precise numerical equality is implied; rather, $R_{\rm corr}$ marks the radius beyond which the effective mixed–state description ceases to evolve in the manner assumed in Equation (14).

Notably, highly dynamical or non–stationary environments (e.g. violent cluster mergers) fall outside this regime because the density operator $\rho(R,t)$ cannot be treated as quasi–static. The mechanism is therefore not claimed to apply to such systems.

It is instructive to contrast this behaviour with MONDian frameworks. In MOND, flat rotation curves arise from a modification of the force law below a universal acceleration scale a_0, and additional prescriptions—such as the external field effect—are required to regulate asymptotic behaviour. In the present approach, neither Newtonian gravity nor Einstein's equations are modified. The saturation of the effective contribution emerges instead from the finite domain of validity of the QCLT coarse–grained description, rendering the theory intrinsically self–limiting.

In ΛCDM, flat rotation curves are attributed to extended dark–matter halos whose density profiles are constrained phenomenologically and truncated at the virial radius. The present framework achieves

 doi:10.20944/preprints202603.1532.v1

a similar phenomenology over galactic scales without invoking additional matter components. While ΛCDM requires halo profiles and concentrations as external inputs, the quantum-induced contribution arises directly from the quantum statistical properties of baryonic subsystems and their environment, with saturation determined by the loss of coherence and self–averaging at large radii.

Importantly, the eventual decline of rotation curves beyond $R_{\rm corr}$ is fully consistent with both observational limitations and expectations from standard halo models, and does not conflict with existing rotation–curve data.

6.3. Mass Distribution

Unlike standard MOND, where a universal acceleration scale a_0 is introduced and is independent of structural density, our formulation associates the relevant scale κ with the baryonic mass distribution itself. For an idealised exponential disk [26,27],

$$\Sigma(r) \quad = \quad \Sigma_0 e^{-r/R_d}, \tag{26}$$

where R_d is the disk scale length and Σ_0 the central surface density.

Integrating over r gives the total baryonic mass M_b,

$$M_b \quad = \quad 2\pi \int_0^\infty \Sigma(r)\, r\, dr = 2\pi\Sigma_0 R_d^2, \tag{27}$$

so that

$$R_d = \sqrt{\frac{M_b}{2\pi\Sigma_0}}. \tag{28}$$

We identify the intrinsic scale κ in (9) with this structural scale, up to a dimensionless proportional constant,

$$\kappa \propto R_d \sim \sqrt{\frac{M_b}{\Sigma_0}}. \tag{29}$$

This identification naturally yields several key empirical consequences, when the condition $\kappa \ll R \ll R_{\rm corr}$ is satisfied, within which the asymptotic velocity obeys to leading order:

$$V_{\rm flat} \propto \left(G M_b \sqrt{\frac{\Sigma_0}{M_b}} \right)^{1/2} \propto M_b^{1/4} \Sigma_0^{1/4}. \tag{30}$$

From which,

- The Tully-Fisher relation [28], where the asymptotic velocity obeys $V_{\rm flat} \propto M_b^{1/4}$ (rather than $\propto M_b^{1/2}$ according to Newtonian gravitation) is reproduced. Note that our framework naturally avoids both infinite isothermal halos and external–field sensitivities, while reproducing the baryonic Tully–Fisher relation within the same radial regime where it is empirically defined
- The relation (30) also provides a testable prediction $V_{\rm Flat} \propto \Sigma_0^{1/4}$ against empirical observation
- It also implies that the onset of orbital velocity flattening occurs at smaller radii κ for galaxies with higher central baryonic surface densities Σ_0. Conversely, diffuse, gas-rich disks—with smaller Σ_0—exhibit later flattening, consistent with HI rotation-curve observations [29,30]. These relationships are illustrated schematically in Figure 3. While both MOND and ΛCDM reproduce approximately flat rotation curves, neither framework predicts the radius at which flattening begins from baryonic structure alone. In contrast, within the present framework the onset of flattening emerges naturally when the galactocentric radius exceeds the intrinsic structural scale κ, providing a direct quantification of the observed correlation between disk scale length and the transition to flat rotation curves.

 doi:10.20944/preprints202603.1532.v1

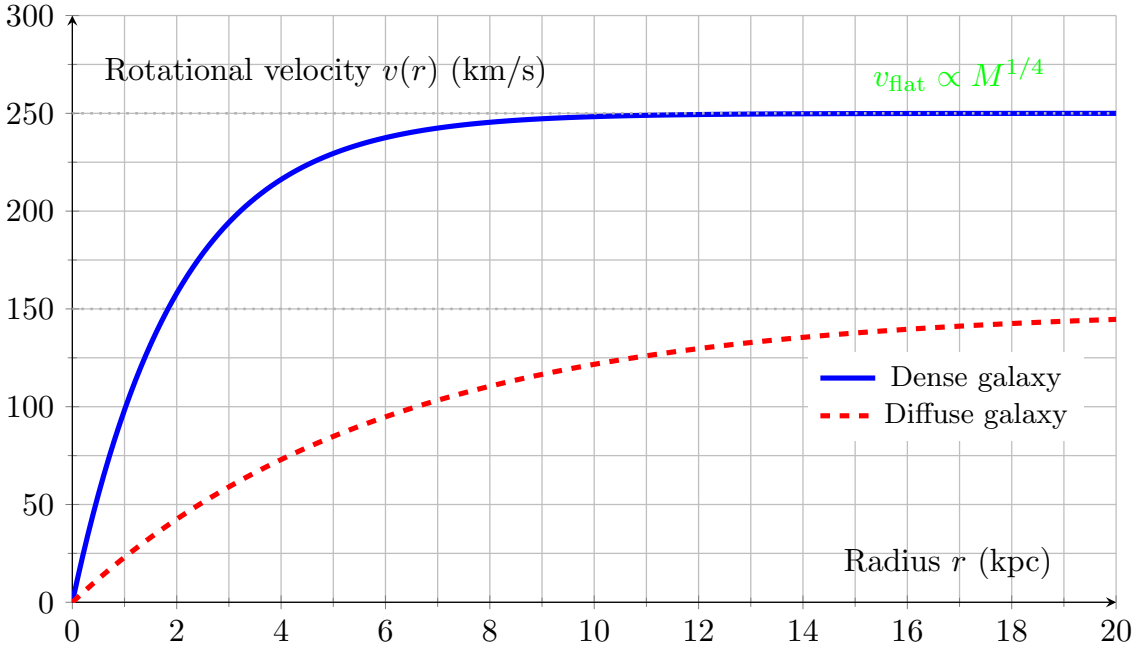

Figure 3. Two stylised galaxy rotation curves, one dense (stellar-dominated) and one diffuse (gas-rich), with different Tully–Fisher asymptotic velocity scalings. That is, the denser galaxy has a larger baryonic mass and therefore a higher asymptotic (flat) velocity. At the same time, the denser galaxy flattens earlier, while the diffuse one flattens later.

6.4. Radial Acceleration Relation RAR

The radial acceleration relation was introduced and studied as an empirical relation in [31]. It was then noted that "The radial acceleration relation appears to be a law of nature, a sort of Kepler's law for rotating galaxies."

Pure Newtonian baryonic radial acceleration is caused by baryonic matter,

$$g_{\text{bar}} = G\,M_b/R^2 \tag{31}$$

A function was introduced which fitted the observed radial acceleration g_{obs} data very well

$$g_{\text{obs}} = \frac{g_{\text{bar}}}{1-e^{-\sqrt{g_{\text{bar}}/g_\dagger}}}, \tag{32}$$

$$\xrightarrow{g_{\text{bar}} \ll g_\dagger} \sqrt{g_\dagger\, g_{\text{bar}}}, \tag{33}$$

with some empirical scale $g_\dagger$. This one-to-one correspondence between g_{bar} and g_{obs} suggests that the baryons are the source of the gravitational potential.

On the other hand, we have from our QCLT framework in Section 4,

$$\begin{aligned} g_{\text{obs}} &\sim g_{\text{bar}}(1+R/\kappa), \\ &\xrightarrow{R\gg\kappa} \sqrt{G\,\Sigma_0}\sqrt{g_{\text{bar}}} \end{aligned} \tag{34}$$

with substitution for $R = \sqrt{G\,M_b/g_{\text{bar}}}$ from (31), and for κ from (29). Thus,

$$\log(g_{\text{obs}}) \rightarrow \log\sqrt{G\,\Sigma_0} + \log\sqrt{g_{\text{bar}}}, \tag{35}$$

cf (33). With a typical spread of about 5 dex for the central surface densities Σ_0 in SPARC, the spread comes from the first term on the rhs of the last expression is about 0.4 dex in systematic shift between galaxy populations. This is consistent with the observed scatter reported in [31]. It predicts that the

 doi:10.20944/preprints202603.1532.v1

RAR is not a universal single curve but a family of curves parameterised by Σ_0, with slope 1/2 in log-log space (same as MOND's interpolation in the low-acceleration limit). This is a genuine and distinguishable prediction. This prediction in the low-acceleration limit is clean and directly testable: plotting $\log(g_{\rm obs}/g_{\rm bar}^{1/2})$ vs. $\log(\Sigma_0)$ for SPARC galaxies should yield a slope of 1/2, which would be a powerful validation.

6.5. Other Non-Relativistic Effects

- *Microscopic Binding Scales:* Because the subsystems may be tightly bound microscopically, one might expect corrections suppressed by powers of λ_b/R, where λ_b is a microscopic length. The present mechanism does not rely on such ratios. The leading correction originates from the radial dependence of mixture weights, $\omega(R) = 1 - c/R$, which generates a macroscopic term

$$\langle 1/r^2 \rangle = \frac{1}{R^2} + \frac{1}{\kappa R} + O(R^{-2}), \tag{36}$$

  independent of microscopic binding lengths.
- *Thermal Effects:* Also, as the QCLT applies equally to mixed states, finite temperature modifies second moments,

$$\sigma_r^2(T) = \sigma_{r,0}^2 + \delta\sigma_r^2(T), \tag{37}$$

  thereby renormalising the scale κ. For dynamically cold neutral hydrogen, velocity dispersions are small compared with orbital velocities, so the linear scaling in R is preserved. A detailed kinetic treatment would refine, but not qualitatively alter, the asymptotic behaviour.
- *Cluster-Scale Behaviour:* Galaxy clusters fall outside the domain of validity of the present framework on two grounds. First, the dominant baryonic component is hot X-ray gas ($kT \sim 5$˜$10keV$), which is dynamically hot and cannot be treated as a large-N ensemble of cold, nearly-identical quantum subsystems. Second, the merger timescale in systems like the Bullet Cluster is much shorter than the decoherence timescale required for the QCLT mixed-state description to be quasi-static. The quasi-dark matter mechanism as presented is therefore not claimed to operate at cluster scales. However, self-consistent mean-field approximation, to take into account those factors, may enable the QCLT framework. Failing that, any residual mass discrepancy there may require a distinct explanation.

6.6. Relativistic Considerations

A fully relativistic treatment—linking the quantum-induced effective potential to spacetime metric perturbations governing null geodesics—is required to assess the compatibility of the present framework with gravitational lensing in galaxies and clusters [32], as well as with the large-scale anisotropy spectrum of the cosmic microwave background (CMB) [33].

While the QCLT does not modify the Einstein field equations, tracing out environmental degrees of freedom introduces an emergent, scale-dependent stress-energy contribution into the semiclassical Einstein equation:

$$G_{\mu\nu} = 8\pi G\left(T_{\mu\nu}^{\rm baryon} + \Delta T_{\mu\nu}^{\rm quantum}\right) \tag{38}$$

To mimic the required dark matter profile, this macroscopic quantum correction $\Delta T_{\mu\nu}^{\rm quantum}$ must structurally behave dynamically as a pressure-less perfect fluid yielding an effective energy density $\Delta T_{00}^{\rm quantum} \propto (\kappa R^2)^{-1}$.

Whether the present mechanism admits a consistent relativistic extension capable of reproducing observed gravitational lensing remains an open problem. No claim is made here regarding lensing or cosmological observables, which require a covariant treatment not developed in this work.

 doi:10.20944/preprints202603.1532.v1

6.7. Laboratory Quantum Systems

It is conceivable that the collective behaviour of a dilute Bose–Einstein Condensate (BEC) might mimic aspects where nonlocal correlations produce effective long-range coherence and modified collective inertia [34,35]. Laboratory observation of analogous scaling relations in controlled BEC systems (with appropriate Feshbach resonance tuning to obtain non-interacting subsystems) could therefore provide indirect tests of the underlying QCLT mechanism (for instance, by engineering an anharmonic optical trap $\Phi(r) = -\gamma/\sqrt{r^2 + d^2}$). Inducing a macroscopic center-of-mass displacement, the Ehrenfest acceleration expands as:

$$\langle \nabla\Phi(\mathbf{r}) \rangle \approx \nabla\Phi(R) + \frac{1}{2}\sigma_r^2 \nabla^3\Phi(R) + \mathcal{O}(\sigma_r^4). \tag{39}$$

Measuring the oscillation frequency shift $\Delta\omega_{\text{dipole}} \propto \sigma_r^2 \nabla^3\Phi(R)$ in the laboratory would provide an indirect, empirical test of the underlying QCLT macroscopic mass scaling.

6.8. Comparison and Testability

We directly compare the main features of various frameworks in Table 1. In the next Table 2, we spell out some testability for QCLT mechanism.

Table 1. Comparison Table.

Criterion	ΛCDM	MOND	QCLT
Assumption	CDM particles	Modified gravity below a_0	Quantum corrections
Flat rotation curves	Dark halos (ad hoc)	Modified dynamics	Induced effective mass (no new particle/fileds)
Onset of flattening	Not predicted	Not predicted	Predicted from $\kappa \propto R_d$
Baryonic Tully–Fisher	Emergent (tuned)	Fundamental	Emergent with factor $\Sigma_0^{1/4}$
Radial Acceleration Relation RAR	Not trivial to achieve	Anticipated	Emergent with factor $\Sigma_0^{1/2}$
Asymptotic behaviour	Virial truncation	External field effect	Saturation beyond R_{corr}
Galaxy clusters	Successful	Needs extra dark component	Undetermined
Gravitational lensing	Natural	Needs relativistic extension	Needs covariant extension
Cosmology / CMB	Successful	Extra assumptions	Not addressed

Table 2. Testability Table.

QCLT outputs	Testability
$V_{\text{flat}} \propto \Sigma_0^{1/4}$	novel, directly testable from SPARC data
Flattening onset, $\kappa \propto \sqrt{M_b/\Sigma_0}$	quantitative, galaxy-by-galaxy testable
Baryonic Tully–Fisher	factor $\Sigma_0^{1/4}$ provides a test against the observed data
RAR, $g_{\text{obs}} \propto \sqrt{G\Sigma_0}\sqrt{g_{\text{bar}}}$	dependency on Σ_0 provides a test against the observed RAR
BEC frequency shift, $\Delta\omega_{\text{dipole}} \propto \sigma_r^2 \nabla^3\Phi(R)$	laboratory analogue test of QCLT macroscopic mass correction

7. Summary and Concluding Remarks

In this work we have explored the consequences of applying the Quantum Central Limit Theorem (QCLT) to macroscopic systems in gravitational fields, and have shown that quantum statistical coarse-graining alone generates an effective additional force that mimics the observational signatures of dark matter over an intermediate radial regime. The analysis proceeds at three levels—a physically transparent Gamma-mixture construction, a minimal single-distribution Inverse Gaussian construction, and a fully general Tweedie framework—all of which converge to the same astrophysical predictions.

Summary of Main Results

The central mathematical result is that for a macroscopic body of $N \gg 1$ identical quantum subsystems in a gravitational potential, the Ehrenfest equation acquires an additional term as in (9), which is strictly positive by Jensen's inequality for any state with non-zero radial variance. No

 doi:10.20944/preprints202603.1532.v1

modification of Newton's law or Einstein's equations is required; the effect is a structural consequence of the nonlinear expectation-value algebra that governs quantum coarse-graining.

The Tweedie generalisation reveals that the radial scaling of this correction is governed by a single parameter, the Tweedie power index p, $\Delta M(R)/M_b \propto R^{p-2}$. The requirement of flat rotation curves uniquely selects $p = 3$—the Inverse Gaussian distribution [20,22,36]. This distribution is independently motivated as the first-passage-time distribution of hydrogen atoms diffusing under Lindblad open-system dynamics in the outer galactic disk [14–16]. The two-component Gamma mixture of Appendix B is formally equivalent to the Inverse Gaussian at leading order.

The astrophysical consequences, derived without introducing new particles or modifying gravity, are as follows.

(i) **Flat rotation curves.** For $\kappa \ll R \ll R_{\rm corr}$, the effective enclosed mass grows as $\Delta M \propto R$, producing a logarithmic potential $\Phi(R) \propto \ln(R/R_0)$ and a constant circular velocity $V_{\rm flat}^2 = GM_b/\kappa$.

(ii) **Effective density profile and potential.** The emergent quasi-dark matter density follows an isothermal profile $\rho_{\rm quasi} \propto R^{-2}$, corresponding to a logarithmic gravitational potential. This profile is *derived* from the quantum statistical structure, not assumed—a significant advantage over both ΛCDM (which inputs halo profiles) and MOND (which modifies dynamics globally).

(iii) **Onset of flattening.** The transition from Keplerian to flat rotation occurs at $R \sim \kappa \propto \sqrt{M_b/\Sigma_0}$: earlier for dense, high-surface-brightness galaxies and later for diffuse gas-rich disks. This galaxy-by-galaxy prediction is absent from both ΛCDM and MOND.

(iv) **Baryonic Tully–Fisher relation.** Identifying $\kappa \propto R_d \propto \sqrt{M_b/\Sigma_0}$ with the exponential disk scale length yields

$$V_{\rm flat} \propto M_b^{1/4}\,\Sigma_0^{1/4},$$

reproducing the observed baryonic Tully–Fisher relation.The additional factor $\Sigma_0^{1/4}$ constitutes a new, testable prediction.

(v) **Radial Acceleration Relation.** In the intermediate regime, the observed and baryonic accelerations satisfy

$$g_{\rm obs} \propto \sqrt{G\Sigma_0}\,\sqrt{g_{\rm bar}},$$

consistent with the empirical RAR, with the Σ_0-dependence of the intercept providing a falsifiable signature distinguishable from the universal interpolation function of MOND.

(vi) **Saturation and Keplerian restoration.** Beyond $R_{\rm corr}$, identified with the HI truncation radius $R_{\rm corr} \sim 4$–$6\,R_d$, the quasi-dark mass saturates to $\Delta M_\infty = M_b R_{\rm corr}/\kappa$ and the rotation velocity returns to Keplerian decline, $V(R) \propto R^{-1/2}$. The mechanism is intrinsica lly self-limiting and requires no external truncation prescription.

Limitations and Open Questions

The present analysis is restricted to non-relativistic, galactic-scale dynamics traced by dynamically cold neutral hydrogen at intermediate radii $\kappa \ll R \ll R_{\rm corr}$. Several important open questions remain.

Relativistic extension. A fully covariant treatment is required to assess compatibility with gravitational lensing [32] and the anisotropy spectrum of the cosmic microwave background [33]. The emergent stress-energy tensor $\Delta T_{\mu\nu}^{\rm quantum}$ must structurally behave as a pressure-less perfect fluid to mimic the required dark matter profile; whether this is consistent with a fully covariant formulation remains open.

Cluster scales. Galaxy clusters fall outside the domain of validity of the present framework: the dominant baryonic component is dynamically hot ($kT \sim 5$–10 keV), violating the cold-subsystem assumption, and cluster merger timescales are shorter than the decoherence timescale required for the quasi-static mixed-state description. Whether a generalised mean-field extension of the QCLT framework can accommodate cluster-scale phenomenology remains to be investigated.

 doi:10.20944/preprints202603.1532.v1

Quantitative confrontation with data. The framework makes concrete, galaxy-by-galaxy predictions for the onset radius κ, the flat velocity $V_{\rm flat}$, and the RAR intercept, all expressible in terms of observable baryonic quantities M_b and Σ_0. A direct fit to rotation curves from the SPARC database, extracting λ as a function of galaxy properties and testing the universality of the proportionality constant in $\kappa \propto \sqrt{M_b/\Sigma_0}$, is the most pressing near-term test of the theory.

Dark energy connection. The saturated logarithmic potential beyond $R_{\rm corr}$ has the character of a locally uniform energy density. In the relativistic extension, the emergent $\Delta T^{\rm quantum}_{\mu\nu}$ may acquire off-diagonal components with a non-trivial equation of state, potentially connecting to the cosmological dark energy density. Whether the QCLT-induced corrections, summed coherently over all baryonic matter in the observable universe, reproduce the observed $\rho_\Lambda \sim 10^{-26}\,\mathrm{kg\,m^{-3}}$ is an open and quantitative question requiring a covariant treatment.

Laboratory analogues. As discussed in Subsection 6.7, dilute Bose–Einstein condensates in anharmonic traps provide a controlled setting in which the QCLT macroscopic mass correction can be probed via dipole oscillation frequency shifts [34,35]. With appropriate Feshbach resonance tuning to achieve non-interacting subsystems, measuring $\Delta\omega_{\rm dipole} \propto \sigma_r^2 \nabla^3 \Phi(R)$ would constitute an indirect empirical test of the underlying mechanism, independent of all astrophysical uncertainties.

Broader Significance

Furthermore, the framework is not unique to gravity. Analogous QCLT-induced corrections may arise for any nonlinear interaction potential $V(r) \propto r^{-n}$, $n \geq 1$, in systems where intra-ensemble correlations can be treated within a self-consistent mean-field description. The Tweedie power index p that selects the physically relevant fixed point will depend on the specific interaction, opening a new programme of inquiry into emergent force-law corrections from quantum coarse-graining across different domains of physics.

Whether quantum-induced effects supplement or supplant particle dark matter remains to be determined. However, the convergence of independent lines of reasoning—the QCLT Jensen correction, and the Inverse Gaussian first-passage-time statistics of open quantum systems—suggests that this mechanism captures something structurally deep about the relationship between quantum statistical mechanics, decoherence, and the large-scale dynamics of the universe.

Acknowledgments: I thank Peter Hannaford and Andrei Sidorov valuable suggestions.

Appendix A. Derivation of a Quantum Central Limit Theorem for Function of a Coarse-Grained/Renormalisation Block Variable

Consider a system with identical and non-interacting components (as in the case of an ideal gas)

$$|\Phi\rangle = \otimes_i^N |\phi_i\rangle,$$

where $|\phi_i\rangle = |\phi\rangle$, for all i.

Now with some function f, we consider

$$\mathcal{E} \quad = \quad \left\langle \Phi \middle| f\left(\frac{1}{N}\sum_i^N \hat{x}_i\right) \middle| \Phi \right\rangle \tag{A1}$$

Insert the resolution of identity into the above

$$\hat{1} = \int \prod_i^N dx_i |x_i\rangle\langle x_i|,$$

where

$$\hat{x}_i|y_i\rangle \quad = \quad y_i|y_i\rangle.$$

 doi:10.20944/preprints202603.1532.v1

Then we have

$$\begin{aligned}\mathcal{E} &= \left\langle \Phi \middle| \left(\int \prod_j^N dy_j |y_j\rangle\langle y_i| \right) \int f\left(\frac{1}{N}\sum_i^N \hat{x}_i \right) \prod_k^N dx_k |x_k\rangle\langle x_k| \middle| \Phi \right\rangle \\ &= \int f\left(\frac{1}{N}\sum_i^N x_i \right) \prod_k^N |\langle x_k|\phi_k\rangle|^2 dx_k \end{aligned} \tag{A2}$$

Insert the identity

$$1 = \int dX\, \delta\left(X - \frac{1}{N}\sum_j^N x_j \right),$$

in which the delta function can be expressed as

$$\delta(u) = \frac{1}{2\pi}\int dw\, \mathrm{e}^{iwu}.$$

We further obtain

$$\begin{aligned}\mathcal{E} &= \int dX \int \delta\left(X - \frac{1}{N}\sum_j^N x_j \right) f\left(\frac{1}{N}\sum_k^N x_k \right) \prod_i^N |\langle x_i|\phi_i\rangle|^2 dx_i, \\ &= \frac{1}{2\pi}\int dX\, dw\, f(X)\, \mathrm{e}^{iXw} \left[\int dx\, \mathrm{e}^{-ixw/N} |\langle x|\phi\rangle|^2 \right]^N, \end{aligned} \tag{A3}$$

It should be emphasised that the probability distributions of the constituents $|\langle x|\phi_i\rangle|^2$ are functions of the time in general; and that, in arriving at (A3), we have had to take the *same* instant of time for all the component probabilities.

$$\begin{aligned}\mathcal{E} &= \frac{1}{2\pi}\int dX\, dw\, f(X)\, \mathrm{e}^{iXw} \left[\int dx\, (1 - iwx/N - w^2x^2/2N^2 + O(1/N^3)) |\langle x|\phi\rangle|^2 \right]^N, \\ &= \frac{1}{2\pi}\int dX\, dw\, f(X)\, \mathrm{e}^{iXw} \left[1 - iw\langle x\rangle/N - w^2\langle x^2\rangle/2N^2 + O(1/N^3) \right]^N, \\ &= \frac{1}{2\pi}\int dX\, dw\, f(X)\, \mathrm{e}^{iXw}\, \exp\{-iw\langle x\rangle - w^2(\langle x^2\rangle - \langle x\rangle^2)/2N + O(1/N^2)\}. \end{aligned} \tag{A4}$$

Integrating over w, we finally arrive at the result

$$\left\langle \Phi \middle| f\left(\frac{1}{N}\sum_i^N \hat{x}_i \right) \middle| \Phi \right\rangle \overset{N\gg 1}{\longrightarrow} \frac{1}{(\sigma_x/\sqrt{N})2\pi\sqrt{2\pi}} \int dX\, f(X) \exp\left\{ -\frac{(X - \langle x\rangle)^2}{2(\sigma_x/\sqrt{N})^2} \right\}, \tag{A5}$$

where in (A4) and (A5), we have defined

$$\langle x\rangle \equiv \int x |\langle x|\phi\rangle|^2 dx = \langle\phi|\hat{x}|\phi\rangle, \tag{A6}$$

$$\sigma_x^2 \equiv \langle x^2\rangle - \langle x\rangle^2. \tag{A7}$$

Similarly, we also have, with some function g,

$$\left\langle \Phi \middle| g\left(\frac{1}{N}\sum_i^N \hat{p}_i/\mu \right) \middle| \Phi \right\rangle \overset{N\gg 1}{\longrightarrow} \frac{1}{(\sigma_p/\sqrt{N})2\pi\sqrt{2\pi}} \int d(P/m)\, g(P/m) \exp\left\{ -\frac{(P/m - \langle p/\mu\rangle)^2}{2(\sigma_p/\sqrt{N})^2} \right\}, \tag{A8}$$

 doi:10.20944/preprints202603.1532.v1

where $m = N\mu$. We have defined

$$\langle p \rangle \equiv \int p |\langle p|\phi\rangle|^2 dp = \langle \phi|\hat{p}/\mu|\phi\rangle, \tag{A9}$$

$$\sigma_p^2 \equiv \langle p^2/\mu^2\rangle - \langle p/\mu\rangle^2. \tag{A10}$$

In the limit $N \to \infty$, the Gaussian functions approach δ functions,

$$\left\langle \Phi \middle| f\left(\frac{1}{N}\sum_i^N \hat{x}_i\right) \middle| \Phi \right\rangle \overset{N\to\infty}{\longrightarrow} f(\langle x\rangle), \tag{A11}$$

$$\langle \Phi | g(\hat{P}/m) | \Phi \rangle \overset{N\to\infty}{\longrightarrow} g(\langle p/\mu\rangle). \tag{A12}$$

Appendix B. Mixture of two Gamma Distributions with Linear Asymptotics

For our subsystem Hamiltonian (4) we have exactly similar mathematics as for the Hydrogen atom, of which the radial components of the energy eigen wave functions can be constructed from the Gamma distributions $\Gamma(r;\alpha,\beta)$

$$\Gamma(r;\alpha,\beta) = \frac{\beta^\alpha}{\Gamma(\alpha)} r^{\alpha-1} e^{-\beta r}, \qquad r > 0. \tag{A13}$$

We consider a quantum mixed state that results in a density of a mixture of two distinct Gamma components.

Let $f_X(r)$ be a density having a mixture of two Gamma components:

$$f_X(r) \sim \omega\,\Gamma(r;\alpha_1,\beta_1) + (1-\omega)\,\Gamma(r;\alpha_2,\beta_2), \tag{A14}$$

with $\alpha_1, \alpha_2 > 2$ so that $\mathbb{E}[1/r^2]$ exists for each component.

For a single Gamma $\Gamma(r;\alpha,\beta)$ one has

$$\mathbb{E}[r] = \frac{\alpha}{\beta}, \qquad \mathbb{E}\left[\frac{1}{r^2}\right] = \frac{\beta^2}{(\alpha-1)(\alpha-2)}.$$

Hence for the mixture

$$\mathbb{E}[r] = \omega\frac{\alpha_1}{\beta_1} + (1-\omega)\frac{\alpha_2}{\beta_2}, \tag{A15}$$

$$\mathbb{E}\left[\frac{1}{r^2}\right] = \omega\frac{\beta_1^2}{(\alpha_1-1)(\alpha_1-2)} + (1-\omega)\frac{\beta_2^2}{(\alpha_2-1)(\alpha_2-2)}. \tag{A16}$$

Let R be the large expectation value for the distance. We want to have

$$\mathbb{E}[r] \overset{R\to\infty}{\longrightarrow} R. \tag{A17}$$

An ansatz for that is to fix the constants

$$\alpha_1, \alpha_2 > 2, \qquad \beta_2 > 0, \qquad c > 0,$$

and define a R-dependent mixture by, for $R > c$,

$$\beta_1(R) = \frac{\alpha_1}{R}, \qquad \omega(R) = 1 - \frac{c}{R}. \tag{A18}$$

The key points are:

- Component 1 (large/bulk): $\Gamma(r;\alpha_1,\beta_1(\mu))$ has mean $\alpha_1/\beta_1(R) = R$
- Component 2 (small/anchor): $\Gamma(r;\alpha_2,\beta_2)$ has fixed, small mean α_2/β_2

 doi:10.20944/preprints202603.1532.v1

- The mixing weight on the small component, which is R-dependent, is $(1-\omega(R)) = c/R$, that is, it is rare for large R

  For this family, we have

$$\mathbb{E}\left[\frac{1}{r^2}\right] = \left(1-\frac{c}{R}\right)\frac{\alpha_1^2/R^2}{(\alpha_1-1)(\alpha_1-2)} + \frac{c}{R}\,\frac{\beta_2^2}{(\alpha_2-1)(\alpha_2-2)}, \tag{A19}$$

from which we can obtain asymptotic expansions for large R:

$$\mathbb{E}[r] \overset{R\gg c}{\longrightarrow} R + o(R), \tag{A20}$$

$$\mathbb{E}\left[\frac{1}{r^2}\right]\mathbb{E}[r]^2 \overset{R\gg c}{\longrightarrow} \frac{\alpha_1^2}{(\alpha_1-1)(\alpha_1-2)} + \underbrace{\frac{c\,\beta_2^2}{(\alpha_2-1)(\alpha_2-2)}}_{1/\kappa} R + o(R), \tag{A21}$$

$$\kappa \coloneqq (\alpha_2-1)(\alpha_2-2)/c\beta_2^2. \tag{A22}$$

The constant term on the rhs of (A21) is an $O(1)$ correction to the effective baryonic mass (renormalising M_b slightly).

Appendix C. The Tweedie Distributions

Appendix C.1. General Quasi-Dark Mass from Tweedie Distributions

We now derive the quasi-dark matter contribution for a general Tweedie subsystem state $\hat{\rho}(R) = \mathrm{Tw}_p(\mu(R),\phi)$, with $\mu(R) = \mathbb{E}[r] \to R$ as required by Equation (14).

Appendix C.1.1. The Jensen Correction via the Delta Method

For any distribution with mean μ and variance $\sigma^2 = \phi\mu^p$, the second-order Taylor expansion (delta method) applied to the convex function $f(r) = 1/r^2$ gives

$$\mathbb{E}\left[\frac{1}{r^2}\right] = \frac{1}{\mu^2} + \frac{3\,\mathrm{Var}(r)}{\mu^4} + O\Big(\mathrm{Var}(r)^2\Big), \tag{A23}$$

where the coefficient of $\mathrm{Var}(r)/\mu^4$ follows from $f''(r)|_{r=\mu} = 6/\mu^4$ and the delta-method formula $\mathbb{E}[f(r)] \approx f(\mu) + \frac{1}{2}f''(\mu)\,\mathrm{Var}(r)$. Substituting the Tweedie variance (17):

$$\mathbb{E}\left[\frac{1}{r^2}\right] = \frac{1}{\mu^2} + \frac{3\phi}{\mu^{4-p}} + O(\phi^2). \tag{A24}$$

The Jensen correction is therefore

$$\mathbb{E}\left[\frac{1}{r^2}\right] - \frac{1}{\langle r\rangle^2} = \frac{3\phi}{\mu^{4-p}} \overset{\mu\to R}{\longrightarrow} \frac{3\phi}{R^{4-p}}. \tag{A25}$$

Note that for $p = 2$ (Gamma), Equation (A25) gives $3\phi/R^2$, which combined with the factor $\langle r\rangle^2 \sim R^2$ in Equation (9) would yield a constant $\Delta M/M_b$ — inconsistent with flat rotation curves. We return to this point in Section C.3 below.

Appendix C.1.2. Emergent Quasi-Dark Mass

Substituting (A25) into the quasi-dark matter expression (9):

$$\frac{\Delta M(R)}{M_b} = \left(\mathbb{E}\left[\frac{1}{r^2}\right] - \frac{1}{\langle r\rangle^2}\right)\langle r\rangle^2 \approx 3\phi\,R^2\cdot R^{-(4-p)} = 3\phi\,R^{p-2}. \tag{A26}$$

 doi:10.20944/preprints202603.1532.v1

This is the central result of this section. The Tweedie power index p directly and uniquely controls the radial scaling of the emergent quasi-dark matter contribution:

$$\boxed{\frac{\Delta M(R)}{M_b} \propto R^{p-2}.} \tag{A27}$$

The corresponding effective density profile follows from $\rho_{\rm quasi}(R) = (4\pi R^2)^{-1}\,\mathrm{d}(\Delta M)/\mathrm{d}R$:

$$\rho_{\rm quasi}(R) \propto R^{p-5}. \tag{A28}$$

Table A1 summarises the physical interpretation of each Tweedie subfamily.

Table A1. Radial scaling of the quasi-dark matter contribution and effective density profile for different Tweedie power indices p. The case $p = 3$ (Inverse Gaussian) is the unique member producing flat rotation curves.

p	Distribution	$\Delta M/M_b$	$\rho_{\rm quasi}$	Rotation curve
$p < 2$	Heavy-tailed	R^{p-2}, declines	$> R^{-3}$	Declining
$p = 2$	Gamma	R^0 = const	R^{-3}	Keplerian†
$p = 3$	Inv. Gaussian	R^1	R^{-2}	**Flat** ✓
$p = 4$	—	R^2	R^{-1}	Rising
$p > 4$	—	R^{p-2}, steep rise	R^{p-5}	Steeply rising

†Single-component Gamma without R-dependent mixture weights; see Section C.3.

Appendix C.1.3. Uniqueness of $p = 3$ for Flat Rotation Curves

The condition for a flat rotation curve is $V^2 = G(M_b + \Delta M)/R = \text{const}$, which requires $\Delta M(R) \propto R$, i.e., $p - 2 = 1$, giving uniquely

$$p = 3 \quad \Longleftrightarrow \quad \text{flat rotation curve.} \tag{A29}$$

Within the Tweedie family, $p = 3$ is the *Inverse Gaussian* distribution. This is not a fine-tuning: it is the unique fixed point of the QCLT coarse-graining map (via the convergence theorem [18]) that is simultaneously consistent with flat galactic rotation curves. The physical content is that the first-passage-time statistics of diffusing hydrogen atoms in the outer galactic disk — described by the Inverse Gaussian — is precisely the distribution that generates an isothermal quasi-dark matter halo.

Appendix C.2. Explicit Construction for $p = 3$: Single Inverse Gaussian

For $p = 3$, the Inverse Gaussian $\mathrm{IG}(\mu, \lambda)$ with $\mu(R) = R$ (so that $\langle r \rangle_\mu \to R$ as required) gives the exact moments:

$$\mathbb{E}[r] = R, \qquad \mathrm{Var}(r) = \frac{R^3}{\lambda}. \tag{A30}$$

For the Inverse Gaussian, $\mathbb{E}[1/r^2]$ is available in closed form. Using the moment-generating function of the Inverse Gaussian [36]:

$$\mathbb{E}\left[\frac{1}{r^2}\right]_{\rm IG} = \frac{1}{R^2} + \frac{3}{\lambda R} + \frac{15}{2\lambda^2} + O\left(R^{-1}\right). \tag{A31}$$

The Jensen correction is:

$$\mathbb{E}\left[\frac{1}{r^2}\right] - \frac{1}{R^2} = \frac{3}{\lambda R} + \frac{15}{2\lambda^2} + \cdots \xrightarrow{R \gg \kappa} \frac{3}{\lambda R}. \tag{A32}$$

Substituting into Equation (9):

$$\frac{\Delta M(R)}{M_b} = \frac{3R^2}{\lambda R} = \frac{3R}{\lambda}. \tag{A33}$$

 doi:10.20944/preprints202603.1532.v1

Appendix C.2.1. Effective Density Profile

From Equation (A33), $\Delta M(R) = M_b R/\kappa$, so:

$$\rho_{\rm quasi}(R) = \frac{1}{4\pi R^2}\frac{{\rm d}(\Delta M)}{{\rm d}R} = \frac{M_b}{4\pi\kappa R^2} \propto R^{-2}, \tag{A34}$$

confirming the isothermal profile, consistent with Equation (15).

Appendix C.2.2. Gravitational Potential

The effective gravitational potential per unit mass corresponding to the total enclosed mass $M_{\rm eff}(R) = M_b(1 + R/\kappa)$ is obtained by integrating $-GM_{\rm eff}(R)/R^2$:

$$\begin{aligned}\Phi(R) &= -\int_R^\infty \frac{GM_{\rm eff}(R')}{R'^2}\,{\rm d}R' \\ &= -\frac{GM_b}{R} - \frac{GM_b}{\kappa}\ln\left(\frac{R_{\rm corr}}{R}\right) + {\rm const}, \qquad \kappa \ll R \ll R_{\rm corr}.\end{aligned} \tag{A35}$$

The second term is the logarithmic potential characteristic of an isothermal halo, and yields the circular velocity:

$$V^2(R) = R\left.\frac{{\rm d}\Phi}{{\rm d}R}\right|_{\rm quasi} = \frac{GM_b}{\kappa} = V_{\rm flat}^2 = {\rm const}, \tag{A36}$$

in agreement with Equation (22).

Appendix C.3. Tweedie Distribution and the Connection to the Gamma Distribution Approach

A careful reader of Appendix B will note an apparent tension: the Gamma distribution ($p = 2$) is used there, yet Table A1 shows that $p = 2$ gives a constant $\Delta M/M_b$, not the linear scaling $\Delta M \propto R$ required for flat rotation curves. This tension is resolved by noting that Appendix B does not use a single Gamma distribution but a *two-component mixture* with an R-dependent weight $\omega(R) = 1 - c/R$.

If we consider only the variance of the Gamma mixture within the delta method (second-order Taylor expansion *approximation*), we run into apparent contradiction with the results of *exact* calculation in Appendix B. The resolution lies in the fact that the delta method is insufficient here: the Gamma mixture has heavy-enough tails that higher-order cumulant contributions to $\mathbb{E}[1/r^2]$ are not negligible for intermediate R. The *exact* calculation in Appendix B (Eqs. B7–B9) uses the closed-form Gamma moments $\mathbb{E}[1/r^2]_\Gamma = \beta^2/[(a-1)(a-2)]$ directly, and the linear $\Delta M \propto R$ arises from the *anchor component's* $\mathbb{E}[1/r^2]_2 = \beta_2^2/[(\alpha_2-1)(\alpha_2-2)]$ weighted by $(1-\omega(R)) = c/R$.

The key insight is the mixture weight promotes $p = 2$ to effective $p = 3$:

> *The Gamma mixture at $p = 2$ achieves the same linear $\Delta M \propto R$ as the Inverse Gaussian at $p = 3$, but requires two components and an R-dependent weight to do so. The Inverse Gaussian achieves this in a single distribution with a parameter λ, because its variance ${\rm Var}(r) = R^3/\lambda$ already scales as μ^3 — precisely the power law that, via the Jensen correction, generates a linear quasi-dark mass.*

Note that the delta method approximation underlying Equation (A23) is valid when $R/\lambda \ll 1$. In the astrophysically relevant regime $\kappa \ll R \ll R_{\rm corr}$ with $R_{\rm corr} \sim$ 4–6 $R_d \sim \kappa$, this condition is marginal. However, the exact asymptotic expansion of $\mathbb{E}[1/r^2]$ for the Inverse Gaussian (Equation (A31)) is valid for all $R \gg \kappa$ and confirms that the linear term $3/\lambda R$ dominates at leading order, with the subleading $15/(2\lambda^2)$ absorbed into the saturation mass ΔM_∞. The result $\Delta M/M_b \propto R$ is therefore exact at leading order in κ/R, not merely a delta-method approximation.

Appendix C.4. Astrophysical Results Under the Tweedie/Inverse Gaussian Framework

Since the Inverse Gaussian ($p = 3$) reproduces $\Delta M(R)/M_b = R/\kappa$ exactly, all astrophysical results of Sections 6 follow without modification.

 doi:10.20944/preprints202603.1532.v1

Appendix C.5. Summary and Hierarchy of Constructions

The relationship between the three levels of construction is as follows.

Level 1 (Appendix B): A two-component Gamma mixture with R-dependent weight $\omega(R) = 1 - c/R$. This is the most explicit and pedagogically transparent construction. It connects directly to hydrogen eigenstate wavefunctions (s-wave, $\ell = 0$) and yields linear $\Delta M \propto R$ through the exact closed-form Gamma moments.

Level 2 (Appendix C.2): A single Inverse Gaussian distribution $\mathrm{IG}(R, \lambda)$ with parameter λ. This is the minimal one-parameter construction achieving the same result. It is motivated by the first-passage-time interpretation of hydrogen atom diffusion under Lindblad decoherence, and eliminates the need for a two-component mixture or an R-dependent weight.

Level 3 (Appendix C.1): The general Tweedie family $\mathrm{Tw}_p(\mu, \phi)$ with $\mu(R) = R$. This is the most general construction, showing that flat rotation curves uniquely select $p = 3$. It provides a structural explanation for why the Inverse Gaussian is the correct distribution: it is not imposed, but selected by the observed astrophysics.

The three constructions are equivalent in the intermediate regime $\kappa \ll R \ll R_{\mathrm{corr}}$ to leading order in R/R_{corr}, and all yield the same astrophysical results. The Tweedie framework thus establishes that the quasi-dark matter mechanism is *robust*: it does not depend on the specific choice of Gamma parameters but is a universal consequence of the $p = 3$, physically realised by the decoherence dynamics of cold hydrogen in the outer galactic disk.

References

1. Cirelli, M.; Strumia, A.; Zupan, J. Dark Matter. *arXiv preprint* **2024**, [2406.01705v3].
2. Milgrom, M. A modification of the Newtonian dynamics as a possible alternative to the hidden mass hypothesis. *Astrophysical Journal* **1983**, *270*, 365–370.
3. Bekenstein, J.; Milgrom, M. Does the missing mass problem signal the breakdown of Newtonian gravity? *Astrophysical Journal* **1984**, *286*, 7–14.
4. Famaey, B.; McGaugh, S.S. Modified Newtonian Dynamics (MOND): Observational phenomenology and relativistic extensions. *Living Reviews in Relativity* **2012**, *15*, 10.
5. Verlinde, E.P. Emergent gravity and the dark universe. *SciPost Physics* **2017**, *2*, 016.
6. Blanchet, L.; Le Tiec, A. Model of dark matter and dark energy based on gravitational polarization. *Physical Review D* **2008**, *78*, 024031.
7. Milgrom, M. The modified dynamics as a vacuum effect. *Physics Letters A* **1999**, *253*, 273–279.
8. Berezhiani, L.; Khoury, J. Theory of dark matter superfluidity. *Physical Review D* **2015**, *92*, 103510.
9. Skordis, C.; Złośnik, T. New relativistic theory for modified Newtonian dynamics. *Physical Review Letters* **2021**, *127*, 161302.
10. Kieu, T.D. Quantum central limit theorems, emergence of classicality and time-dependent differential entropy. *Entropy* **2023**, *25*, 600. https://doi.org/10.3390/e25040600.
11. Tweedie, M.C.K. An index which distinguishes between some important exponential families. In Proceedings of the Statistics: Applications and New Directions. Proceedings of the Indian Statistical Institute Golden Jubilee International Conference; Ghosh, J.K.; Roy, J., Eds., Calcutta, 1984; pp. 579–604.
12. Jørgensen, B. Exponential dispersion models (with discussion). *J. R. Stat. Soc. Ser. B* **1987**, *49*, 127–162.
13. Jørgensen, B. *The Theory of Dispersion Models*; Chapman & Hall: London, 1997.
14. Lindblad, G. On the generators of quantum dynamical semigroups. *Commun. Math. Phys.* **1976**, *48*, 119–130. https://doi.org/10.1007/BF01608499.
15. Gorini, V.; Kossakowski, A.; Sudarshan, E.C.G. Completely positive dynamical semigroups of N-level systems. *J. Math. Phys.* **1976**, *17*, 821–825. https://doi.org/10.1063/1.522979.
16. Arnold, A.; Fagnola, F.; Neumann, L. Quantum Fokker–Planck models: the Lindblad and Wigner approaches. In *Quantum Probability and Related Topics*; World Scientific, 2008; Vol. 23, *QP–PQ: Quantum Probab. White Noise Anal.*, [arXiv:0804.2551].
17. Frank, T.D. *Nonlinear Fokker–Planck Equations: Fundamentals and Applications*; Springer: Berlin, 2005. https://doi.org/10.1007/b137680.
18. Jørgensen, B.; Martínez, J.R.; Tsao, M. Asymptotic behaviour of the variance function. *Scand. J. Stat.* **1994**, *21*, 223–243.

 doi:10.20944/preprints202603.1532.v1

19. Dunn, P.K.; Smyth, G.K. Series evaluation of Tweedie exponential dispersion model densities. *Stat. Comput.* **2005**, *15*, 267–280. https://doi.org/10.1007/s11222-005-4070-y.
20. Schrödinger, E. Zur Theorie der Fall- und Steigversuche an Teilchen mit Brownscher Bewegung. *Physikalische Zeitschrift* **1915**, *16*, 289–295.
21. von Smoluchowski, M. Notiz über die Berechnung der Brownschen Molekularbewegung bei der Ehrenhaft-Millikanschen Versuchsanordnung. *Physikalische Zeitschrift* **1915**, *16*, 318–321.
22. Seshadri, V. *The Inverse Gaussian Distribution*; Oxford University Press: Oxford, 1993.
23. Begeman, K.G.; Broeils, A.H.; Sanders, R.H. Extended rotation curves of spiral galaxies: Dark haloes and modified dynamics. *Monthly Notices of the Royal Astronomical Society* **1991**, *249*, 523–537.
24. Sofue, Y.; Rubin, V. Rotation curves of spiral galaxies. *Annual Review of Astronomy and Astrophysics* **2001**, *39*, 137–174.
25. McGaugh, S.S. Predictions and outcomes for the dynamics of gas-rich galaxies. *Galaxies* **2020**, *8*, 35.
26. Freeman, K.C. On the disks of spiral and S0 galaxies. *Astrophysical Journal* **1970**, *160*, 811.
27. Mo, H.J.; Mao, S.; White, S.D.M. The formation of galactic disks. *Monthly Notices of the Royal Astronomical Society* **1998**, *295*, 319–336.
28. Tully, R.B.; Fisher, J.R. New method of determining distances to galaxies. *Astronomy and Astrophysics* **1977**, *54*, 661.
29. Lelli, F.; et al. The baryonic Tully–Fisher relation for a sample of 153 galaxies. *Astrophysical Journal* **2019**, *872*, 88.
30. McGaugh, S.S.; et al. Dynamical regularities in galaxies. *Astronomical Journal* **2021**, *162*, 202.
31. McGaugh, S.S.; Lelli, F.; Schombert, J.M. Radial Acceleration Relation in Rotationally Supported Galaxies. *Phys. Rev. Lett.* **2016**, *117*, 201101. https://doi.org/10.1103/PhysRevLett.117.201101.
32. Clowe, D.; et al. A direct empirical proof of the existence of dark matter. *Astrophysical Journal Letters* **2006**, *648*, L109.
33. Planck Collaboration. Planck 2018 results. VI. Cosmological parameters. *Astronomy & Astrophysics* **2020**, *641*, A6.
34. Pitaevskii, L.P.; Stringari, S. *Bose–Einstein Condensation*; Clarendon Press, 2003.
35. Carusotto, I.; Ciuti, C. Quantum fluids of light. *Reviews of Modern Physics* **2013**, *85*, 299.
36. Folks, J.L.; Chhikara, R.S. The inverse Gaussian distribution and its statistical application—a review. *J. R. Stat. Soc. Ser. B* **1978**, *40*, 263–289.